PROPAGATION OF SPIN WAVES IN NANOSCALE BONDED FERRITE FILMS

© 2025 V. V. Balaeva*, D. V. Romanenko, M. A. Morozova

Saratov State University, Saratov, Russia

**e-mail: vkonda2000@mail.ru*

Received November 14, 2024
Revised December 03, 2024
Accepted December 30, 2024

Abstract. Using micromagnetic modeling methods the propagation of spin waves in two nanoscale laterally bonded ferrite films was studied. The features of the power pumping of surface and backward volume magnetostatic waves are investigated. The effect of the distance between the films and the films' width of the films on the pumping length and cutoff frequency of these types of waves has been established.

Keywords: *spintronics, spin wave, magnetostatic waves, pumping, YIG, ferrite, nanomaterial, micromagnetic modeling, coupled structure, lateral structure*

DOI: 10.31857/S03676765250426e2

INTRODUCTION

In recent years, micro- and nanostructures based on magnetic materials have attracted wide interest of researchers due to their potential use in next-generation communication systems, where information will be transmitted using magnons or spin waves [1, 2].

Spin waves and their magnon quanta are promising information carriers in future signal processing systems because the Hilbert attenuation associated with the propagation of spin waves can be significantly reduced compared to Joule heat losses

in electronic devices. A number of concepts of magnetic logic and signal processing on spin waves have been proposed [3, 4]. But one of the unsolved problems of magnetic technology is the efficient and controllable coupling of individual magnetic signal processing devices into a magnetic circuit. For this purpose, coupled structures are promising candidates. Coupled structures significantly expand the functional capabilities of radio-physical systems, since an additional control parameter - coupling - appears. Such structures are widely used both in microwave engineering [5, 6] and in optical systems [7, 8]. In the case of two coupled waveguide ferromagnetic structures, coupling leads to the appearance of symmetric and antisymmetric normal waves propagating with different group and phase velocities, whose characteristics can be controlled by changing the distance between the coupled waveguides [9]. Due to the coupling between magnetic channels, the dynamical properties of wave processes change significantly and new types of spin excitations are realized [10, 11].

Two types of coupled magnon systems can be distinguished, namely waveguides arranged in planar geometry, parallel [12, 13] and at an angle to each other [14, 15] (transversely coupled waveguides), and waveguides having the form of multilayer structures [16, 17]. For the realization of controlled coupling between magnon channels, planar geometry is more relevant, since experimental studies of sandwich structure are rather difficult due to the lack of access to individual layers, which is necessary for excitation and reception of propagating CBs.

Earlier studies of the peculiarities of wave propagation in planar-transversely coupled structures were carried out using Brillouin light scattering for micron-thick films [12, 13] and microwave methods for micro- and nanoscale ferromagnetic films

[12, 18]. It has been demonstrated that such systems realize periodic power transfer from one waveguide to another, and the spatial period can be controlled by the magnitude of the permanent magnetic field, the orientation of the static magnetization of the channels, and the geometry of the coupled structure [18, 19]. Most of the works are devoted to consideration of micron-sized structures. However, modern technologies for growing magnetic films make it possible to create films of nanoscale thickness, which is more relevant from the point of view of miniaturization and energy efficiency of devices on such structures.

In [20], the propagation of CBs in laterally coupled nanoscale magnetic waveguides for the case of inverse bulk magnetostatic waves (IBWM) is considered. The pumping of OOMSWs between magnetic waveguides was investigated and a waveguide configuration for which a signal tap function based on such a system can be realized was proposed. However, to obtain a complete picture and to conclude about the effectiveness of coupled structures for the realization of magnononic couplings, it is necessary to consider also the case of surface magnetostatic waves (SMW).

In the present work, two types of PMSW and OOMSW waves in laterally coupled nanoscale magnetic waveguides are considered on the basis of micromagnetic modeling using the MuMax3 environment. The features of power pumping between waveguides for both types of spin waves are investigated. The influence of waveguide geometry, including waveguide width and waveguide spacing, on the character of spin wave pumping is investigated.

PROBLEM MODEL AND RESEARCH METHODS

Fig. 1a shows a schematic of the investigated structure, which is two ferromagnetic films (FFs) of thickness *S* and width *w*, arranged in planar geometry in one plane. The FPs are separated by an air gap of width *d*. The structure is placed in an external magnetic field of strength H_0. If the field is directed along the *y-axis,* PMSVs propagate in the structure; if the field is directed along the *x-axis*, the inverse PMSVs propagate in the structure. The signal is fed to the input of FP-1.

The structure parameters are as follows: film thickness S = 100 nm, film length L = 100 μm, film width d at least 2 μm, excitation stripe width w = 2 μm. The material parameters of the LIGs are as follows: exchange constant A_{ex}= 3.614·$^{e(-12)}$J/m, saturation magnetization M_{sat}= 1.39·$^{e(5)}$A/m, Hilbert attenuation constant α_G= 0.0001.

The MuMax3 micromagnetic modeling environment solves temporal and spatial problems of magnetization evolution on micro- and nanometer scales. To solve the problems, MuMax3 applies the finite difference method in space, which is partitioned into a three-dimensional grid. The Landau-Lifshitz equation is used to describe the forced oscillations of the magnetization vector. The processing of simulation results was implemented in the Matlab environment using programs and built-in modules.

Let us consider the basic algorithms for solving the problem of magnetostatic wave propagation in a medium MuMax3 .

First, the parameters for the calculations and the required values are set.

1) On all *x, y, z* axes*, the* number and corresponding size of cells are set. In order not to take into account the exchange interaction, the condition$\lambda \gg a_p$, (where) a_p is the lattice constant in the direction of spin wave propagation.

2) If necessary, boundary conditions and attenuation layers are specified.

3) The properties of the medium and field, such as attenuation magnitude, exchange constant, saturation magnetization, magnitude and direction of the external magnetic field, are specified.

The task is divided into two stages: static and dynamic. At the static stage, the initial direction of magnetization in the substance of the structure is set and the *"relax"* command is started. As a consequence, an external field is applied to the sample, under the action of which the magnetization vectors $\overline{M}$ begin to precess and line up with the external field $\overline{H_0}$. The resulting state of the magnetics is used as a stationary state in the subsequent modeling.

At the dynamics stage, excitation by a dynamic magnetic field $\overline{h}$, directed perpendicularly to the external field, is added. The amplitude of the dynamic field in the linear case obeys the condition $\overline{h} \ll \overline{H_0}$. Forcing excitation by the field $\overline{h}$ is set in the form of imposing a "mask" on the region of the waveguide acting as an excitation strip. It is necessary to set the shape of electromagnetic radiation and the shape of the pulse.

Variable Field Function:

$$B = \cos^2(x - x_1) \cdot \cos^2(x - x_2), \tag{17}$$

where x_1 and x_2 are the beginning and end of the excitation strip, respectively.

The momentum function for the excitation mask $F(f_c, t)$ depends on the method of solving the problem, where f_c is the cutoff frequency.

Calculation of spatial distribution of magnetization

The spatial distribution of the dynamic magnetization allows us to consider the dynamics of spin wave propagation, in particular, the period of signal pumping in the coupled structure. From the theory of coupled waves [6], the expression of the pumping length in the case of identical films in terms of parameters takes the form of a periodic function. For convenience in determining the pumping length, let us define the excitation pulse in the following form:

$$I = A \cdot \sin(2\pi f_c t), \tag{18}$$

where A is the pulse amplitude, f_c is the cutoff frequency.

The cutoff frequency f_c is selected using dispersion curves so that the horizontal line at this frequency intersects the symmetric and antisymmetric branches of the desired mode.

At the edges of the structure along the wave direction (*x-axis*), layers with higher attenuation than in the wave propagation medium are set up, increasing towards the edges.

In the process of calculations, we will keep the coordinate of the dynamic magnetization vector $\Delta\overline{m}(x, y, z, t)$, corresponding to one of the axes perpendicular to the external field direction. However, we do not keep the modulus of both perpendicular coordinates (z and y), because in the confined sample the precession is elliptical, not circular. For our calculations, we will choose the z coordinate perpendicular to the external field in the case of both OOMSV and PMSV. We will keep the magnitude corresponding to the deviation of the dynamic magnetization from its stationary state by the z coordinate.

To qualitatively observe the propagation of a spin wave along the *x-axis*, we need the distribution of $\Delta\overline{m}(x,y,z,t)$ in the *xy* plane at a fixed slice height along the *z-axis*. The expression of the magnitude has the form:

$$\Delta m_z(x,y,t) = m_z(x,y,t) - m_z(x,y,0). \tag{19}$$

The data are taken with the time period Δt = 10 ns, the coordinates of cells *x, y, z* and their corresponding value $\Delta m_z(x,y,t)$ are saved in the data file. Thus, we can plot in Matlab the distribution of $\Delta m_z(x,y,t)$ in the plane at time $n\Delta t$, where *n is* an integer. For a smoother view of the $\Delta m_z(x,y,t)$ distribution, we apply the Hilbert transform to the data set.

Calculation of dispersion characteristics

To calculate the variance, the cutoff frequency f_c for the excitation pulse must be selected above the upper threshold of the MSW frequencies. To effectively excite all frequencies below f_c , the function sinc(*x*), which is the inverse Fourier transform for a rectangular pulse, is used. The excitation pulse has the form:

$$I = A \cdot \mathrm{sinc}(2\pi f_c(t - t_0)), \tag{20}$$

where *A* is the pulse amplitude, $t_0$is the initial time.

The spin wave propagates along the *x-axis*, so let us set periodic boundary conditions along this axis.

In the process of calculations, we will keep one of the coordinates of the dynamic magnetization vector $\Delta\overline{m}(x,y,z,t)$. For our calculations, we will choose the *z*

coordinate perpendicular to the external field in the case of both OOMSV and PMSV. Thus, we will keep the value . $\Delta m_z(x,y,z,t)$

Since the width of the films is limited, the internal field includes demagnetization fields, so the value of $\Delta m_z(x,y,z,t)$ should be kept to a narrow three-dimensional slice along the centerline of the film.

The coordinates of cells *x, y, z* and their corresponding value $\Delta m_z(x,y,z,t)$ are stored in the data file. The data are taken with a time period inverse to the sampling frequency F_s.

According to Kotelnikov's theorem, the sampling period of the signal should be chosen from the condition:

$$T = \frac{1}{2f_m}, \tag{21}$$

where f_m is the upper limit of the spectrum of the original signal, for our calculations it is the cutoff frequency f_c . The sampling frequency $F_s$is a multiple of the inverse of the sampling period.

The obtained data set is processed in Matlab environment. Two-dimensional Fast Fourier Transform (FFT) is performed to obtain dispersion curves [21]:

$$m_z(k_x,f) = \frac{1}{N}\sum_{i=1}^{N}\left|\mathbb{F}_2\left[\Delta m_z(x_i,y_i,z,t)\right]\right|^2, \tag{22}$$

where $\mathbb{F}_2$ is the two-dimensional FFT, y_i is the *i-th* cell along the waveguide width, and *N* is the total number of cells along the waveguide width. To visualize the dispersion curve, we construct a 3D color map of $P(k_x,f) \propto \Delta m_z(k_x,f)$ at a logarithmic scale.

Calculation of amplitude-frequency characteristics

As in the case of variance construction, we need to determine the cutoff frequency above the upper cutoff frequency for the MSW. To effectively excite all frequencies below f_c we use the function sinc(x) in the form of expression (20).

At the edges of the structure along the wave direction, attenuation layers are set up as in the algorithm for the magnetization distribution.

In the process of calculations, two values are saved to the data file with sampling rate (21): the time moment t, and the corresponding value $\Delta m_z(x, y, z, t)$ - component along the *z-axis*.

The obtained data are processed in Matlab environment using built-in tools for plotting the AFC, which utilizes one-dimensional Fourier transform.

RESULTS OF MICROMAGNETIC MODELING

Fig. 1 (b) shows the dispersion characteristic for OOMSV in the

of the investigated structure. The dispersion curves corresponding to the first five thickness modes of the structure are plotted, each of which is split into two curves corresponding to symmetric and antisymmetric normal modes of the coupled structure with wave numbers $k_s$and k_{as}, respectively. The existence of symmetric and antisymmetric normal modes for a layered coupled structure has been shown theoretically, for example, in [6, 22]. The propagation of two normal modes in the coupled structure with different phase and group velocities leads to periodic power pumping between the films. The spatial period of pumping (pumping length) in this case is determined by the relation [5, 6]:

$$\Lambda = 2\pi / \left| k_s - k_{as} \right| . \quad (23)$$

Fig. 1c,d shows the amplitude-frequency characteristics (AFC) of the OOMSV and PMSV at the output of FP-1 (blue curve) and FP-2 (red curve). The figures show a sequence of maxima and minima of the FP-1 and FP-2 transfer coefficient, located in opposite phase. This feature indicates power pumping between the films, the length of which is determined by the signal frequency. Theoretical dependencies for the transmission coefficients illustrating the maxima and minima located in antiphase were calculated in [23] for PMSV in coupled micron-thick lateral waveguides. The noted behavior of the transmission coefficients allows us to consider the investigated structure as a functional element for frequency separation of signals. From the comparison of Fig. 1c and Fig. 1g, it can be seen that in the case of OOMSV the waves are effectively coupled at high frequencies, i.e., as can be seen from Fig. 1 (b) at small wave numbers (large wavelengths), and in the case of PMSV - at low frequencies, i.e., also at small wave numbers (large wavelengths). The range of frequencies at which the waves are effectively coupled expands as the distance between the waveguides decreases.

Fig. 2a shows a map of the distribution of the deviation of the dynamic magnetization vector $\Delta m_z(x, y, t)$ in the plane of the waveguides during OOMSV propagation. A series of alternating magnetization maxima and minima in each waveguide along the propagation direction x can be seen. The maxima and minima in FP-1 and FP-2 are located in antiphase, indicating periodic power pumping between the films along the propagation direction. We define the pumping length Λ as the

distance between neighboring maximum values of $\Delta m_z(x,y,t)$ in one film, as shown in Fig. 2a. Since it is important to analyze the periodicity of power pumping between the films, we will take the values of $\Delta m_z(x,y,t)$ only along the center line of each film, where the demagnetization fields are minimal. Fig. 2b shows the dependence of the magnetization deviation in FP-1 (blue curve) and in FP-2 (red curve) on the longitudinal *x* coordinate. The graph also shows maxima and minima in FP-1 and FP-2 alternating in counter-phase, which indicates power pumping between the waveguides. The amplitude of the maxima decreases along the propagation direction, which is due to losses in the ferromagnetic medium.

Fig. 3 shows the dependences of the pumping length on the film gap *d* for different types of waves. For both OOMSV (Fig. 3a) and PMSV (Fig. 3b), the dependence $\Lambda(d)$ is nonlinearly increasing. In each plot, the dependences for different film widths *w* are collected. It can be seen that the pumping length is proportional to the width of the films *w*: for any gap value *d,* the value of the pumping length is larger the larger the width of the films. It can also be seen that the pumping length for PMSV is larger than the pumping length for OOMSV, other parameters being equal. Fig. 3c shows the dependence of the pumping length difference for PMSV and for OOMSV $\Lambda_{ПМСВ} - \Lambda_{ООМСВ}$ on the film width *w* for different film spacing *d*. It can be seen that the pumping length difference increases both with increasing waveguide width and with increasing film width.

Fig. 4 presents the dependences of the cutoff frequency of the first mode of MSW (f' , marked in Fig. 1b) on the value of the gap *d* between the FPs. The results are

shown for two types of waves, PMSW (a) and OOMSW (b), respectively, at different values of the film width *w*. It can be seen that the coupling in the system has a negligible effect on the cutoff frequency, however, the dynamics are different for PMSW AND OOMSW. For OOMSV, the cutoff frequency increases with increasing gap width *d*, while it decreases for PMSV . When the waveguide width w increases, the cutoff frequency decreases for the case of OOMSV and increases for PMSV. Note that in [24] it was shown for PMSV in a single waveguide that the cutoff frequency also increases with increasing waveguide width.

CONCLUSION

On the basis of micromagnetic modeling in the MuMax3 environment, the peculiarities of propagation of surface and inverse bulk magnetostatic waves in nanosized laterally coupled ferrite waveguides are investigated. The amplitude-frequency characteristics, dispersion characteristics, and evolution of magnetization amplitude along the wave propagation direction are calculated. It is shown that in the case of OOMSV the waves are effectively bound at high frequencies, and in the case of PMSV - at low frequencies, i.e., in both cases at long wavelengths. The range of frequencies at which the waves are effectively coupled expands as the distance between the waveguides decreases. It is found that the power transfer length between waveguides increases as the distance between the waveguides increases. When the width of the waveguides increases, the pumping length also increases. It is shown that the pumping length depends on the type of MSW. When the width of the waveguides increases, the pumping length for PMSVs becomes longer than that for OOMSVs, and

the difference in pumping lengths increases as the width of the waveguides increases. The increase is also observed when the gap between the waveguides increases. The effect of coupling between the waveguides on the frequency of cutoff is investigated. The distance between the waveguides has an insignificant effect on the cutoff frequency, however, for OOMSV the dependence is increasing and the cutoff frequency decreases with increasing waveguide width, while for PMSV it is decreasing and the cutoff frequency increases with increasing waveguide width.

The obtained results allow us to consider the investigated structure as a functional element for frequency separation of signals, a power divider, as well as an effective element of interconnections in a magnon network.

FUNDING

This work was supported by the Russian Science Foundation (grant No. 23-29-00759).

REFERENCES

1. *Mahmoud A., Ciubotaru F., Vanderveken F. et al.* // J. Appl. Phys. 2020. V. 128. Art. No. 161101.
2. *Chumak A. V., Kabos P., Wu M. et al.* // IEEE Trans. Magn. 2022. V. 58. P. 1.
3. *Wei D., Xie L., Lee K.K. et al.* // Nature Commun. 2013. V. 4. Art. No. 1374.
4. *Lavrijsen, R., Lee J.Y., Fernández-Pacheco A. et al.* // Nature. 2013. V. 493. P. 647.
5. *Luisell W.* Bound and parametric oscillations in electronics. MOSCOW: IL, 1963. 352 c.
6. *Vashkovsky A.V., Stalmakhov V.S., Sharaevsky Y.P.* Magnetostatic Waves in Microwave Electronics. Saratov: Izd. of Saratov University, 1993. 311 c.
7. *Kivshar Y.S., Agrawal G.P.* Optical solitons. Moscow: Fizmatlit, 2005. 648 c.
8. *Agrawal G.P.* Lightwave Technology: Telecommunication Systems. John Wiley & Sons, Inc., Hoboken, New Jersey. 2005. 480 p.

9. *Nikitov S.A., Tailhadesand P., Tsai C.S.* // J. Magn. Magn. Mater. 2001. V. 236. P. 320.
10. *An K., Bhat V.S., Mruczkiewicz M. et al.* // Phys. Rev. Appl. 2019. V. 11. No. 3. Art. No. 034065.
11. *Wang Q., Pirro P., Verba R. et al.* // Sci. Adv. 2018. V. 4. No. 1. Art. No. e1701517.
12. *Sadovnikov A.V., Odintsov S.A., Beginin E.N.et al.* // Phys. Rev. B. 2017. V. 96. Art. No. 060481(R)
13. *Sadovnikov A.V., Grachev S.A., Beginin E.N. et al.* // Phys. Rev. Appl. 2017. V. 7. Art. No. 014013.
14. *Klingler S., Pirro P., Brächer T. et al.* // Appl. Phys. Lett. 2015. V. 106. Art. No. 212406.
15. *Vogt K., Fradin F.Y., Pearson J.E. et al.* // Nature Commun. 2014. V. 5. P. 3727.
16. *Zelent M., Tobik J., Krawczyk M. et al.* // Phys. Status Solidi. RRL. 2017. V. 11. No. 10. Art. No. 1700259.
17. *Mruczkiewicz M., Graczyk P., Lupo P. et al.* // Phys. Rev. B. 2017. V. 96. Art. No. 104411.
18. *Wang Q., Pirro P., Verba R. et al.* // Sci. Adv. 2017. V. 4. Art. No. e1701517.
19. *Sadovnikov A.V., Beginin E.N., Morozova M.A. et al.* // Appl. Phys. Lett. 2016. V. 109. Art. No. 042407.
20. *Chumak A.V., Serga A.A., Hillebrands B.* // Nature Commun. 2014. V. 5. P. 4700.
21. *Kumar D., Dmytriiev O., Ponraj S., Barman A.* // J. Phys. D. Appl. Phys. 2012. V. 45. Art. No. 015001.
22. *Sasaki H., Mikoshiba N.* // Electron. Lett. 1979. V. 15. P. 172.
23. *Castera J.P., Hartemann P.* // Electron. Lett. 1980. V. 16. P. 195.
24. *O'Keeffe T.W., Patterson R.W.* // J. Appl. Phys. 1978. V. 49. P. 4886.

FIGURE CAPTIONS

Fig. 1. Schematic of the structure based on laterally coupled ferrite films showing two types of propagating MSW: the field along the *x-axis* is OOMSW, along the *y-axis* -

PMSW (a). Dispersion characteristic of OOMSV in the coupled structure (b). Amplitude-frequency characteristics for OOMSV (c) and PMSV (d) at the output of FP-1 (blue curve) and FP-2 (red curve). Calculated parameters: $w = 2$ μm, $d = 1$ μm.

Fig. 2. Spatial distribution of the magnetization deviation $\Delta m_z(x, y, t)$ in the xy plane at fixed z for OOMSV (a). Dependence of the magnetization deviation taken along the center line of each film on the x coordinate (b). Calculated parameters: $w = 2$ μm, $d = 1$ μm.

Fig. 3. Dependences of the pumping length on the distance between the films d at different film widths w for OOMSV (a) and PMSV (b). Dependence of the difference of the pumping lengths of PMSV and OOMSV on the film width w and at different gap width d (c).

Fig. 4. Dependences of the first mode cutoff frequency of OOMSV (a) and PMSV (b) on the gap width d at different values of the film width w.

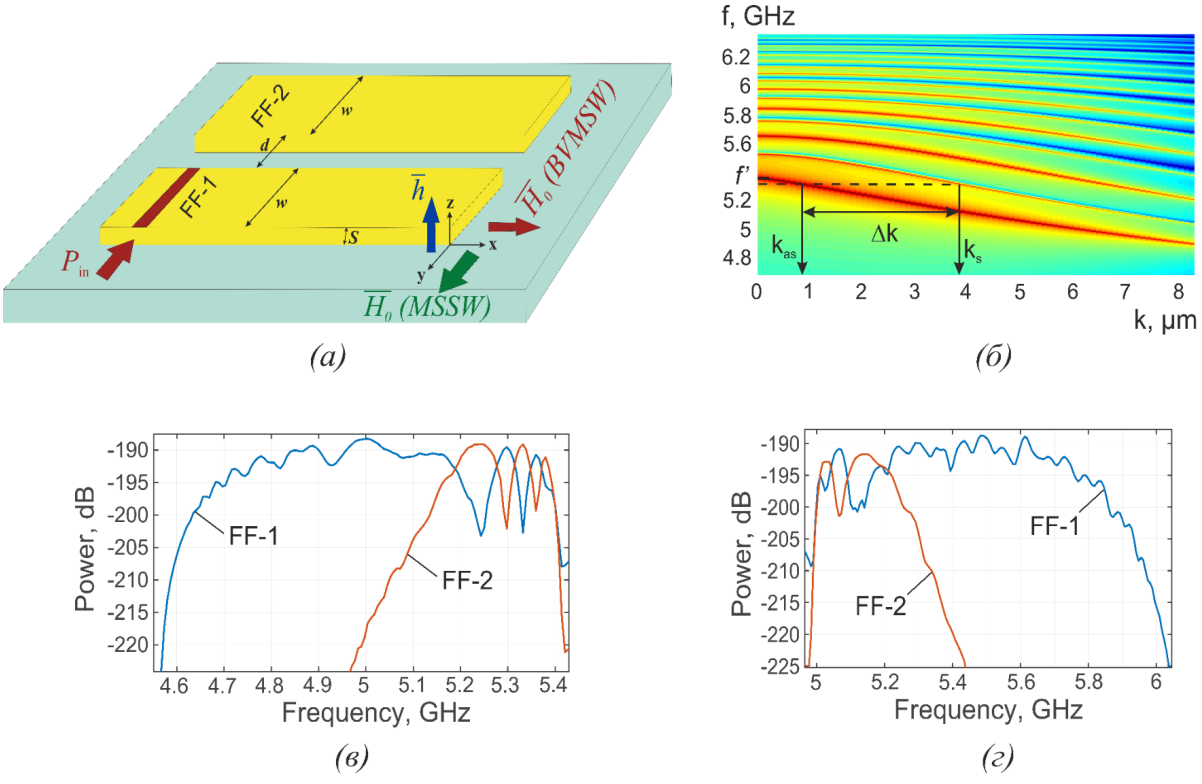

Fig. 1

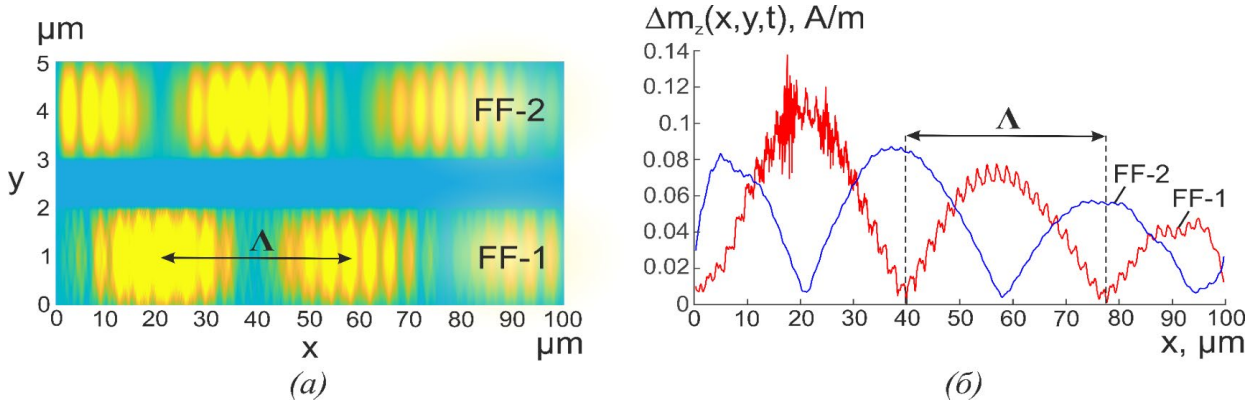

(а) *(б)*

Fig. 2

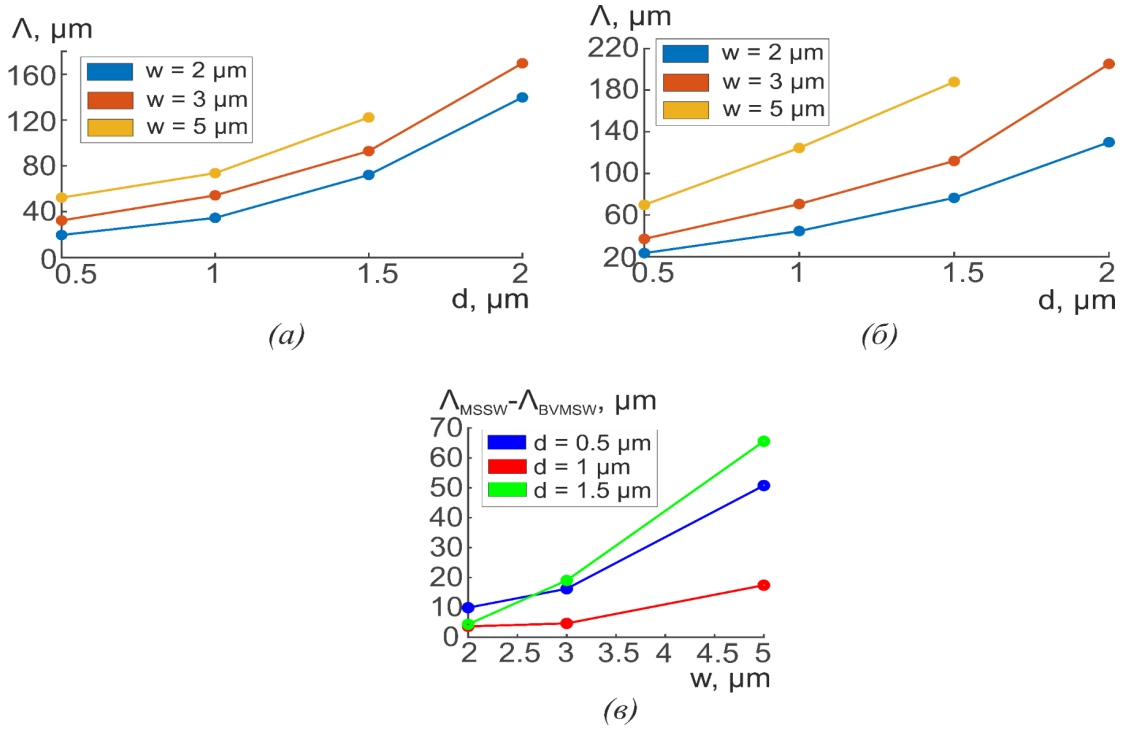

(а) *(б)* *(в)*

Fig. 3

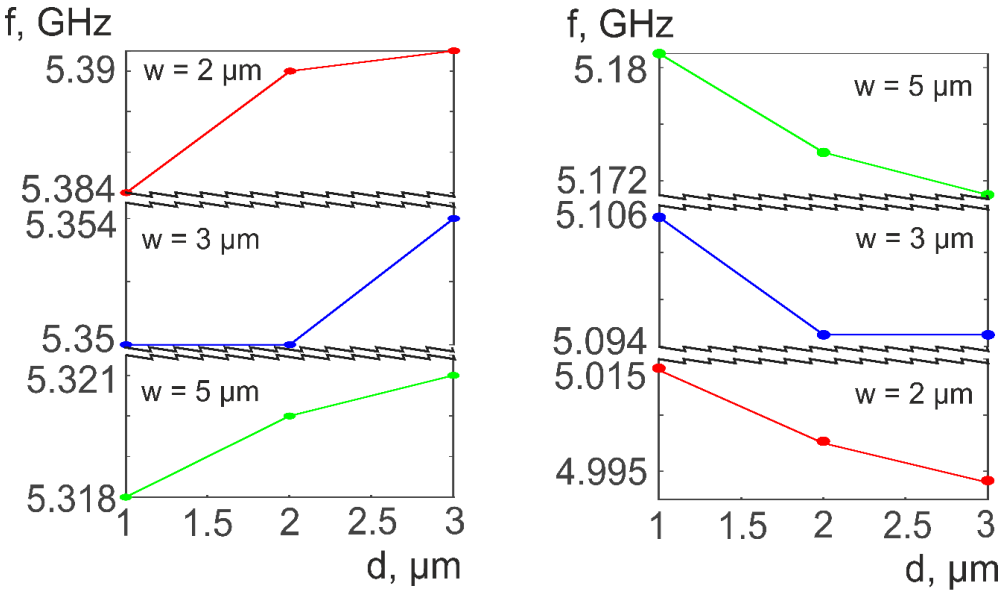
f, GHz
5.39
5.384
5.354
5.35
5.321
5.318
w = 2 μm
w = 3 μm
w = 5 μm
1
1.5
2
2.5
3
d, μm
f, GHz
5.18
5.172
5.106
5.094
5.015
4.995
w = 5 μm
w = 3 μm
w = 2 μm
1
1.5
2
2.5
3
d, μm

(a) *(б)*

Fig. 4